

Projection of temperature and radiation in arid and semi-arid climates under shared socioeconomic pathways scenarios

Marzieh Bagheri Khaneghahi ¹, Aboutaleb HezarJaribi ^{2*}, Mohammad Ismaeil Kamali ³, Fatemeh Zamani ⁴

¹ PhD student in irrigation and drainage engineering, Department of Water Engineering, Faculty of Water and Soil, Gorgan University of Agricultural Sciences and Natural Resources, Gorgan, Iran

² Associate Professor, Department of Water Engineering, Faculty of Water and Soil, Gorgan University of Agricultural Sciences and Natural Resources, Gorgan, Iran

³ Assistant Professor, Soil and Water Research Department, Mazandaran Agricultural and Natural Resources Research and Education Center, AREEO, Sari, Iran

⁴ Assistant Professor, Artificial Intelligence Department, Faculty of Electrical and Computer Engineering, Babol Noshirvani University of Technology, Babol, Iran

Abstract

The phenomenon of climate change, caused by both anthropogenic and natural factors, makes the forecasting of future climate and its impact on the proper management of agriculture, water, and soil resources, as well as watershed management, the environment, and desertification control, crucial. Accordingly, this study investigates future temperature and solar radiation in arid (Mashhad and Ahvaz) and semi-arid (Kermanshah) climates in Iran. First, daily climatic data for the baseline period (1991-2020) were obtained from synoptic stations in the study areas. Subsequently, temperature and solar radiation projections were generated for the future periods of 2021-2040, 2041-2060, and 2061-2080 using LARS-WG version 8, based on the HadGEM3 climate model under the SSP scenarios. The model's high accuracy in downscaling and its excellent performance in predicting climatic parameters across all stations were validated by high R^2 values (99%) and NS efficiency coefficient (99%), alongside low RMSE values (less than 30%). Results indicated that, compared to the 30-year baseline period, the average maximum temperature over the next 60 years is projected to increase by 0.37, 1.48, and 2.73°C (Mashhad); 1.09, 1.47, and 2.3°C (Ahvaz); and 1.3, 1.75, and 2.65°C (Kermanshah) under the SSP126, SSP245, and SSP585 scenarios, respectively. Similarly, the average minimum temperature is expected to rise by 1.01 °C, 1.89 °C, and 2.8 °C (Mashhad); 1.57 °C, 2.17 °C, and 3.24 °C (Ahvaz); and 1.8 °C, 2.43 °C, and 3.33 °C (Kermanshah), respectively. However, changes in mean annual solar radiation did not show a consistent pattern. The monthly trends for temperature and radiation were significant at a 95% confidence level for most months. The results suggest that future temperature increases may lead to a decline in the quantity and quality of agricultural products, reduced water resources, and increased soil erosion. Future changes in solar radiation will also affect photosynthesis, evapotranspiration, energy production, and fossil fuel consumption. Therefore, to mitigate the negative impacts and adapt to future climatic conditions in the study areas, managers and planners should adopt optimal strategies. These strategies include cultivating heat- and light-resistant crops, optimizing irrigation systems, designing watershed management systems to prevent water loss, and promoting sustainable land development.

Keywords: Climate, Downscaling, SSP scenarios, Water and soil resources, HadGEM3.



Article Type: Research Article

*Corresponding Author, E-mail: hezab10@yahoo.com

Citation: Bagheri Khaneghahi, M., HezarJaribi, A., Kamali, M. I., and Zamani, F. (2025). Projection of Temperature and Radiation in Arid and Semi-Arid Climates under Shared Socioeconomic Pathways (SSP) Scenarios. *Water and Soil Management and Modelling*, 5(Special Issue: Climate Change and Effects on Water and Soil), 32–48.
doi: 10.22098/mmws.2025.17004.1568

Received 22 June 2025., Received in revised form: 26 June 2025, Accepted: 27 June 2025., Published online: 29 June 2025
Water and Soil Management and Modeling, , Year 2025, Vol. 5, Special Issue, pp. 32-48.

Publisher: University of Mohaghegh Ardabili

© Author(s)



1. Introduction

In recent decades, the increase in greenhouse gases resulting from the use of fossil fuels, human activities, and land use has led to global warming and climate change. Climate change can manifest differently at the regional scale, leading to extreme and unprecedented weather events with significant changes in their duration and intensity (Clarke et al., 2022; Leydson & Dantas, 2022; Lionello & Scarascia, 2018). Climate change can have a severe impact on various aspects of the environment and numerous fundamental sectors of the global economy, including water and soil resources, agriculture, energy production, and tourism (Al-Kekey et al., 2022; Osman et al., 2014). According to the IPCC's Sixth Assessment Report, the global average temperature is likely to reach or exceed 1.5°C between 2030 and 2050. Rising temperatures increase evapotranspiration and the atmosphere's water-holding capacity. As a result, this can lead to changes in the magnitude, duration, and frequency of precipitation, as well as alterations in its spatial and temporal distribution. Therefore, the increased occurrence of hazards such as droughts and/or floods, driven by rising temperatures and/or declining precipitation, is expected to be one of the primary consequences of global climate change (Mahmoudi & Rigi Chahi, 2019; Dai, 2011; Trenberth et al., 2014). The occurrence of these phenomena can lead to greater aridity in Iran's arid and semi-arid climates, resulting in the loss of agricultural soils, reduced ecosystem productivity, destruction of forests and rangelands, loss of specific plant and animal species, desertification, and increased movement of shifting sands (Mosayyebi, 1996).

To determine the impacts of global warming and assess climate change, General Circulation Models (GCMs) are utilized. These models are widely recognized as the primary tools for understanding historical climate patterns, simulating future climate scenarios, and assessing their impacts (Navarro-Racines, 2020).

GCMs utilize the complexity of the global system to produce valuable results. However, due to their coarse spatial resolution, their direct application in sustainable resource management at regional or local scales is limited (Manwar, 2022; Araya et al., 2021). The two most commonly used

downscaling techniques are statistical downscaling and dynamical downscaling. These two methods refine the coarse-resolution variables from GCMs to the local scale (Tang et al., 2016). CMIP6, the Coupled Model Intercomparison Project Phase 6, is a component of global climate change studies conducted by the Intergovernmental Panel on Climate Change (IPCC) to provide policymakers and researchers with information. It enables the climate science community to evaluate the performance of various models and develop projections and scenarios related to climate change. Compared to its previous versions, CMIP6 includes more advanced and sophisticated climate models (Zamani et al., 2020; Chen et al., 2020). The LARS-WG model is used to downscale the outputs of General Circulation Models (GCMs) and is capable of projecting future climate conditions using limited observational data. This model has been reported to be superior to other models, such as the Statistical Downscaling Model (SDSM) (Semenov & Barrow, 2002). The basis of this model for simulating wet and dry spells, daily precipitation, and radiation series is a semi-empirical distribution composed of 23 intervals. In this model, the Fourier series is used to estimate temperature (Semenov & Stratonovich, 2009). The Shared Socioeconomic Pathways (SSPs) are a set of climate scenarios that define the socioeconomic factors underlying climate change scenarios. The SSPs (from the Sixth Assessment Report) are an update of the RCPs (from the Fifth Assessment Report) and describe future conditions based on five fundamental pathways: sustainability (SSP1), a middle-of-the-road approach (SSP2), regional rivalry (SSP3), inequality (SSP4), and fossil-fueled development (SSP5) (Iranshahi et al., 2022).

Previous research indicates that climate models successfully simulate climatic components, such as temperature and radiation, across various geographical locations and accurately illustrate climate change trends in future periods relative to the past. Zohrevandi et al. (2020) utilized climate scenarios in the LARS-WG software to examine future changes in temperature and radiation across the provinces of Kurdistan, Kermanshah, and Hamedan. They showed that, compared to the

baseline period, radiation, maximum temperature, and minimum temperature would increase by 0.38 MJ/m²/day, 3.3°C, and 3.4°C, respectively. Shoja and Hamidianpour (2024) reported that on the coasts of Kish Island, the mean temperature would increase from a baseline of 25.27 °C to 29.63 °C and 30.33 °C under the SSP2-4.5 and SSP5-8.5 scenarios, respectively, for the 2050-2069 period. The results of a study in a watershed in northern Iraq showed that the highest increases in maximum and minimum temperatures under RCP8.5 for the future period of 2081-2100 were 5.7 °C in July and 5.30 °C in September, respectively (Mohaisen Nasser et al., 2024). Given that climate models are continually being updated and that the investigation of future changes in specific climatic parameters in certain

cities of Iran has been limited, this study aims to project temperature and radiation in arid and semi-arid climates under the Shared Socioeconomic Pathways (SSP) scenarios. For this purpose, LARS-WG8 software was used.

2. Materials and Methods

2.1. Study Area:

The study areas in this research are the Mashhad and Ahvaz stations, which have arid climates, and the Kermanshah station, which has a semi-arid climate. The geographical coordinates, along with the annual mean temperatures and precipitation levels, for the study stations are presented in Table 1. Furthermore, the geographical locations of the study areas are shown on a map of Iran in Figure 1.

Table 1- Characteristics of the studied synoptic stations (Source: National Meteorological Organization)

Study areas	Mashhad	Ahvaz	Kermanshah
Longitude	59.54	48.71	47.07
Latitude	36.32	31.34	34.32
Height above sea level (m)	1027	20	1351
Average annual precipitation (mm)	237.71	210.09	409.33
Average annual temperature (°C)	15.9	26.58	15.56

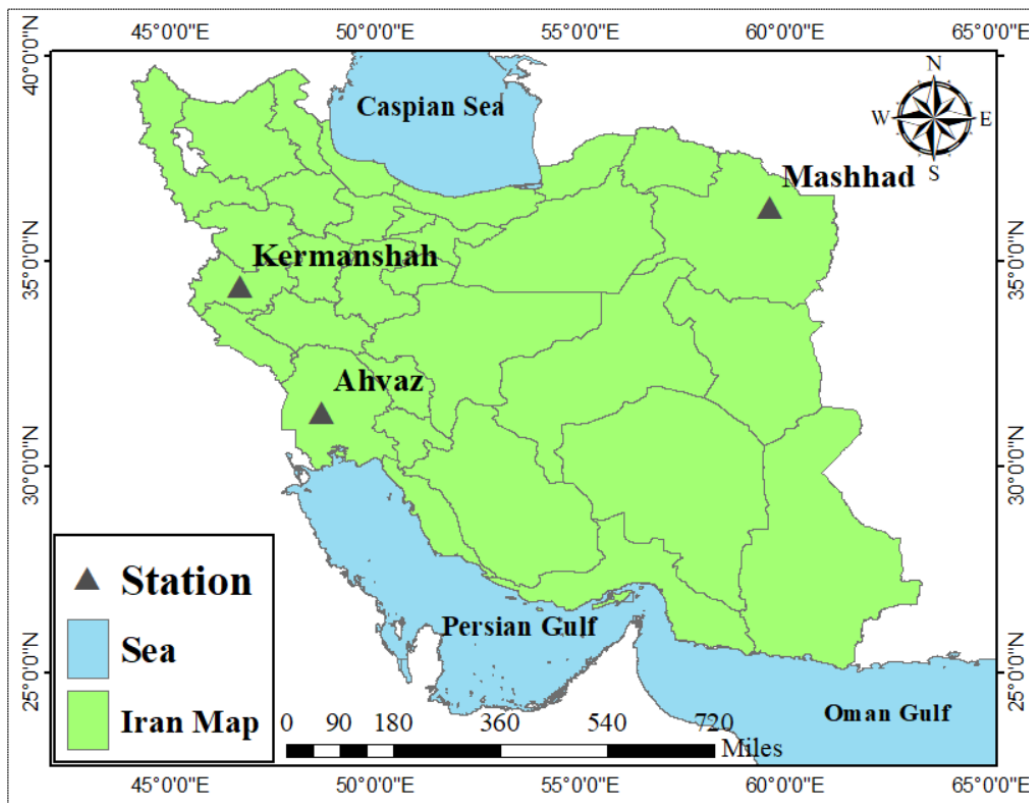


Figure 1- Geographical location of the studied synoptic stations (Mashhad, Ahvaz, and Kermanshah) in Iran

2.2. Research Tools

This research employed the LARS WG8 software, the HadGEM3 climate model, and the SSP1-2.6, SSP2-4.5, and SSP5-8.5 scenarios to project climate parameters, specifically temperature and radiation, across the study regions. The SSP1-2.6 scenario is considered an optimistic scenario, postulating that atmospheric radiative forcing will stabilize at 2.6 W/m². The intermediate scenario, SSP2-4.5, assumes that radiative forcing will remain at 4.5 W/m². The SSP5-8.5 scenario is regarded as a pessimistic scenario; it maintains radiative forcing at 8.5 W/m² and corresponds to the highest levels of emissions and the most adverse climate outcomes (Qin et al., 2022; Haider et al., 2023).

2.3. Methodology

Initially, the daily temperature and radiation dataset for the statistical period from 1991 to 2020 was obtained from the synoptic stations of Mashhad, Ahvaz, and Kermanshah. Subsequently, a text file containing the climatic dataset (structured by year, month, and day) and another text file with information on geographical coordinates (longitude, latitude, and altitude) and CO₂ concentration (based on the software's default value) were created for the study stations and imported into the LARS WG8 software. First, the climate model type was selected from the Generator window of the LARS software, and then the text files were loaded via the Site Analysis window.

In this study, the accuracy of the HadGEM3-GC31-LL climate model within the LARS WG8 software was first evaluated. The model's accuracy was assessed on a monthly basis by comparing observational data (Source: Iran Meteorological Organization) with the modeled data for the historical period (available in the software's database). The statistical indices used in this research were the coefficient of determination (R^2), the Nash-Sutcliffe efficiency (NSE), and the Root Mean Square Error (RMSE) (Equations 1-3). In these equations, O_i and P_i represent the observed and modeled values, respectively; \bar{O} and \bar{P} are their mean values, and n is the number of observations.

$$R^2 = \frac{[\sum_{i=1}^n (P_i - \bar{P})(O_i - \bar{O})]^2}{\sum_{i=1}^n (P_i - \bar{P})^2 \sum_{i=1}^n (O_i - \bar{O})^2} \quad (1)$$

$$NS = 1 - \frac{\sum_{i=1}^n (O_i - P_i)^2}{\sum_{i=1}^n (O_i - \bar{O})^2} \quad (2)$$

$$\text{the RMSE} = \sqrt{\frac{\sum_{i=1}^n (O_i - P_i)^2}{n}} \quad (3)$$

After validating the model's accuracy, the software was executed according to the selected scenarios (SSP126, SSP245, and SSP585) and the chosen future statistical periods (2021-2040, 2041-2060, and 2061-2080) from the corresponding window. The daily maximum temperature, minimum temperature, and radiation data for the future were then extracted as text files.

Finally, the daily parameters from the historical period (1991-2020) and the projected parameters for the first future period (2021-2040), the second future period (2041-2060), and the third future period (2061-2080) were averaged annually in Excel. This was performed by first calculating the mean for each year within a statistical period and then computing the overall average of all years for that specific period. The monthly averaging of parameters was conducted similarly: for the historical period, the parameters were first averaged monthly for each year. Then, all months of the same name from the historical period were averaged together. This process was also performed for each of the future periods.

Thus, graphs of the annual changes in temperature and radiation across the different periods were plotted, and the trend of these changes from the past into the future was evaluated. Furthermore, the trend of monthly changes in the climatic parameters was analyzed using the non-parametric Mann-Kendall test, with the Z-statistic and p-value, in SPSS software. This test was initially introduced by Mann (1945) and was later expanded and developed by Kendall (1975) based on the ranking of data in a time series. In the Mann-Kendall test, the null hypothesis states that the data are random and exhibit no trend, while the alternative hypothesis (the rejection of the null) indicates the existence of a trend in the data series. The Z-statistic is used to measure the presence of a trend in a time series and generally determines whether a trend exists by comparing it to a standard normal distribution. The p-value, in turn, reports the significance of the trend,

which was assessed in this study at a 95% confidence level.

3. Results and Discussion

3.1. Model Accuracy Assessment

The results of the HadGEM3-GC31-LL model's accuracy assessment, based on the statistical indices of the coefficient of determination (R^2), Nash-Sutcliffe efficiency (N-S), and Root Mean Square Error (RMSE) for predicting climatic parameters in the study areas, are presented in

Table 2. In this study, the high R^2 values (0.99) and low RMSE values (less than 0.3) for the climatic parameters indicate the model's high accuracy in downscaling and its excellent agreement across the study areas.

Finally, the projections of annual and monthly averages for the climatic parameters—maximum temperature, minimum temperature, and radiation—based on the HadGEM3 climate model (under scenarios SSP126, SSP245, and SSP585) were discussed and analyzed for the study areas.

Table 2- Accuracy assessment results of the HadGEM3 climate model in predicting climate variables in the study areas

study area	R^2			N-S			RMSE		
	Tmax	Tmin	Ra	Tmax	Tmin	Ra	Tmax	Tmin	Ra
Mashhad	0.99	0.99	0.99	0.99	0.99	0.99	0.27	0.26	0.15
Ahvaz	0.99	0.99	0.99	0.99	0.99	0.99	0.27	0.16	0.17
Kermanshah	0.99	0.99	0.99	0.99	0.99	0.99	0.22	0.21	0.17

3.2. Projection of Maximum Temperature, Minimum Temperature, and Radiation

3.2.1. Mashhad Station

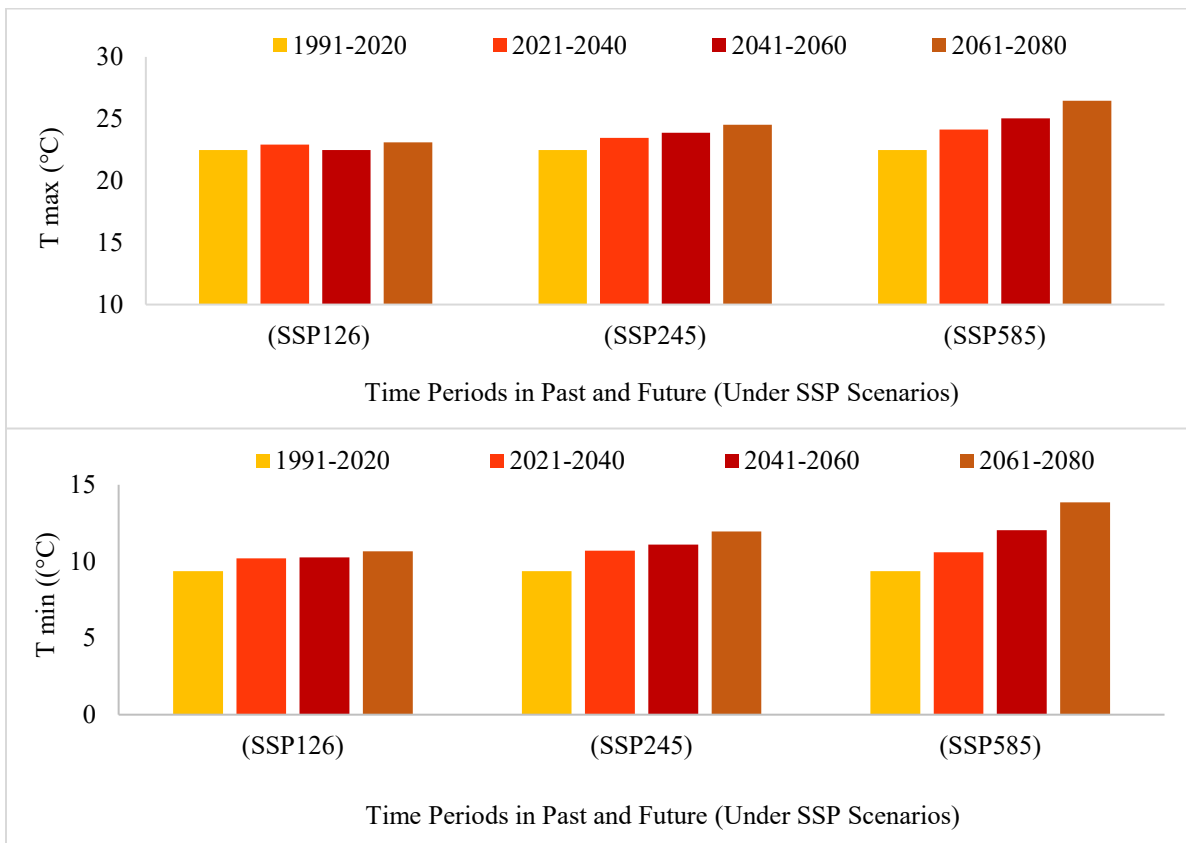
The annual average of maximum temperature, minimum temperature, and radiation for the historical period and future periods under the SSP scenarios for the Mashhad station are presented in Figure 2. In general, the annual average maximum temperature in the future periods under all SSP scenarios is higher than that of the historical period (22.47 °C). For the future periods, under the SSP126 scenario, the annual average maximum temperature, in ascending order, corresponds to the second (22.49 °C), first (22.92 °C), and third (23.11 °C) periods. However, the annual average maximum temperature under the SSP245 scenario, in ascending order, corresponds to the first (23.45 °C), second (23.87 °C), and third (24.53 °C) future periods. Additionally, the annual average maximum temperature under the SSP585 scenario, in ascending order, corresponds to the first (24.14 °C), second (25.03 °C), and third (26.45 °C) future periods. The average maximum temperature for the future 60-year period under the SSP126, SSP245, and SSP585 scenarios is projected to be 0.37 °C, 1.48 °C, and 2.73 °C higher, respectively, than that of the 30-year historical period.

Overall, the annual average minimum temperature in the future periods under all SSP scenarios is higher than that of the historical period (9.36 °C). For the coming periods, under the SSP126 scenario, the annual average minimum temperature, in ascending order, corresponds to the first (10.19 °C), second (10.27 °C), and third (10.66 °C) periods. The annual average minimum temperature under the SSP245 scenario, in ascending order, corresponds to the first (10.7 °C), second (11.1 °C), and third (11.9 °C) future periods. Additionally, the annual average minimum temperature under the SSP585 scenario, in ascending order, corresponds to the first (10.6 °C), second (12.03 °C), and third (13.85 °C) future periods. The average minimum temperature for the coming 60-year period under the SSP126, SSP245, and SSP585 scenarios is projected to be 1.01 °C, 1.89 °C, and 2.8 °C higher, respectively, than that of the 30-year historical period.

When comparing the historical period and the future periods (under the SSP126 scenario), the annual average radiation, in ascending order, corresponds to the second future period (29.03 J/cm²/day), the third future period (29.35 J/cm²/day), the first future period (29.5 J/cm²/day), and the historical period (29.59 J/cm²/day). In a comparison between the historical period and the future periods (under the

SSP245 scenario), the annual average radiation, in ascending order, corresponds to the second future period (29.45 J/cm²/day), the third future period (29.47 J/cm²/day), the historical period (29.59 J/cm²/day), and the first future period (29.76 J/cm²/day). In a comparison between the historical period and the future periods (under the SSP585 scenario), the annual average radiation, in ascending order, corresponds to the third future period (29.57 J/cm²/day), the historical period (29.59 J/cm²/day), the second future period (29.75 J/cm²/day), and the first future period (30.14 J/cm²/day). The average radiation for the future 60-year period is projected to be 0.29 and

0.035 J/cm²/day lower under the SSP126 and SSP245 scenarios, respectively, and 0.23 J/cm²/day higher under the SSP585 scenario, compared to the 30-year historical period. Overall, the total solar energy that arrives at a specific surface within a given timeframe is slightly altered during its passage through the atmosphere. It also experiences local variations depending on factors like the Sun's altitude (solar angle), duration of exposure, changes in cloud cover, total atmospheric mass, concentration of atmospheric components, and the characteristics of the Earth's surface cover.



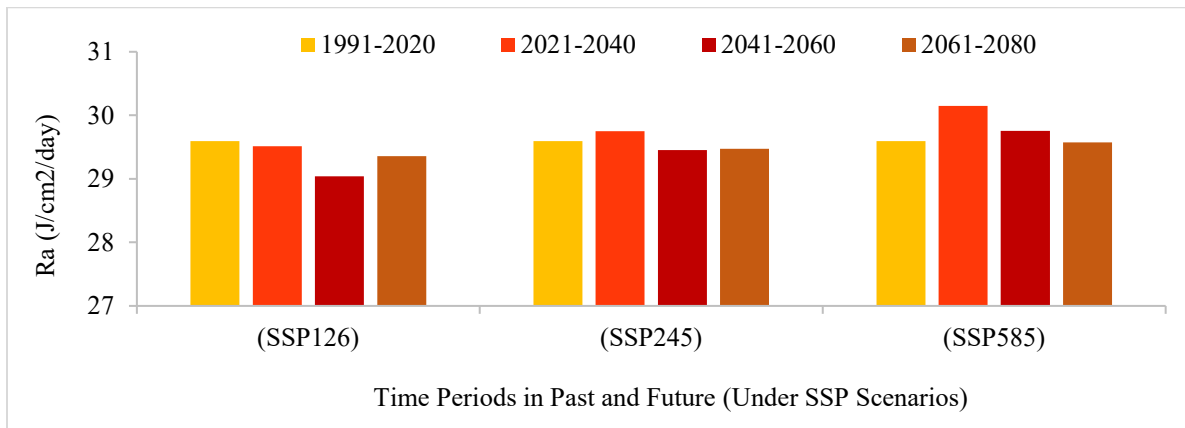


Figure 2. Trends in annual mean maximum temperature, minimum temperature, and solar radiation over historical and future periods (under SSP scenarios) in Mashhad

Table 3 illustrates the trend of changes in the monthly average of climatic parameters, temperature, and radiation at the Mashhad station using the Mann-Kendall non-parametric test. Since the p-values for the maximum and minimum temperature parameters are less than 0.05, the results indicate a statistically significant increasing trend for all months of the year at a 95% confidence level. In a comparison between the historical and future periods (under SSP scenarios), the monthly average maximum and minimum temperatures are higher in the future periods than in the historical period for almost all months.

When comparing the maximum temperature of the historical period with the future periods (under the SSP126, SSP245, and SSP585 scenarios), the highest maximum temperature is observed in July of the third future period (36.26, 37.32, and 39.02 °C, respectively), while the lowest maximum temperature occurs in January of the first future period (8.43, 7.99, and 8.5 °C,

respectively). When comparing the minimum temperature of the historical period with the future periods (under the SSP126, SSP245, and SSP585 scenarios), the highest minimum temperature is found in July of the third future period (21.74, 23.2, and 24.85 °C, respectively). The lowest minimum temperature is observed in January of the historical period (-1.87 °C). Sarabi et al. (2020) demonstrated in a study in Mashhad that both minimum and maximum temperature values are projected to increase in all future periods and under all scenarios compared to the baseline period.

Changes in radiation are statistically significant at the 95% confidence level only for February, March, May, and July. However, for the other months, as the p-values are greater than 0.05, no significant trend is observed. The trend of monthly radiation changes at this station for the future periods, compared to the historical period, does not follow a regular pattern.

Table 3- Analysis of Monthly Trends in Climatic Parameters: Comparison of Future and Historical Periods in Mashhad Using the Non-parametric Mann-Kendall Test

Month	Tmax		Tmin		Ra	
	p-Value	Z	p-Value	Z	p-Value	Z
Jan	0.022	0.234	0.043	0.201	0.074	0.174
Feb	0.017	0.244	0.034	0.212	0.043	0.234
Mrc	0.017	0.234	0.034	0.201	0.022	0.217
Apr	0.022	0.234	0.043	0.234	0.031	0.201
May	0.022	0.212	0.022	0.234	0.043	0.174
June	0.034	0.212	0.022	0.234	0.074	0.174
July	0.022	0.234	0.017	0.244	0.031	0.212
Aug	0.017	0.244	0.022	0.234	0.082	0.168
Sep	0.022	0.234	0.017	0.245	0.082	0.168

Oct	0.022	0.245	0.017	0.245	0.043	0.201
Nov	0.017	0.245	0.022	0.234	0.053	0.19
Dec	0.017	0.234	0.022	0.234	0.053	0.19

3.2.2. Ahvaz Station

Figure 3 shows the annual average of maximum temperature, minimum temperature, and radiation for the historical period and the future periods under the SSP scenarios for the Ahvaz station. In general, the annual average maximum temperature in the coming periods under all SSP scenarios is higher than that of the historical period (33.76 °C).

In the future periods, under the SSP126 scenario, the annual average maximum temperatures, in ascending order, correspond to the first (34.42 °C), second (34.90 °C), and third (35.24 °C) periods, respectively. Under the SSP245 scenario, the annual average maximum temperatures, in ascending order, correspond to the first (34.15 °C), second (35.37 °C), and third (36.19 °C) future periods, respectively. Similarly, under the SSP585 scenario, the annual average maximum temperatures, in ascending order, correspond to the first (34.58 °C), second (36.04 °C), and third (37.64 °C) future periods, respectively. The average maximum temperature in the coming 60-year statistical period under the SSP126, SSP245, and SSP585 scenarios is 1.09, 1.47, and 2.3 °C higher, respectively, than in the historical 30-year statistical period.

In general, the annual average minimum temperature in the future periods under all SSP scenarios is higher than that of the historical period (19.41 °C). In the coming periods, under the SSP126 scenario, the annual average minimum temperatures, in ascending order, correspond to the first (20.62 °C), second (21.09 °C), and third (21.24 °C) periods, respectively. Under the SSP245 scenario, the annual average minimum temperatures, in ascending order, correspond to the first (20.70 °C), second (21.53 °C), and third (22.52 °C) future periods, respectively. Similarly, under the SSP585 scenario, the annual average minimum temperatures, in ascending order, correspond to the first (21.14 °C), second (22.52 °C), and third (24.30 °C) future periods, respectively. The average minimum temperature in the coming 60-year period under the SSP126, SSP245, and

SSP585 scenarios is 1.57, 2.17, and 3.24 °C higher, respectively, than in the historical 30-year statistical period.

In a study conducted in northern Khuzestan, Hajivand Paidari et al. (2022) also used the HadCM model under the A2 and B1 scenarios for the periods of (2011-2030) and (2030-2050). They demonstrated that the most significant temperature increase was related to the minimum temperature and also occurred under the A2 scenario for the 2050 horizon.

When comparing the historical period with the future periods (under the SSP126 scenario), the annual average radiation values, in ascending order, correspond to the first future period (30.94 Joules/cm²/day), the historical period (31.09 Joules/cm²/day), the second future period (31.26 Joules/cm²/day), and the third future period (31.4 Joules/cm²/day). When comparing the historical period with the future periods (under the SSP245 scenario), the annual average radiation values, in ascending order, correspond to the first future period (30.66 Joules/cm²/day), the second future period (31.049 Joules/cm²/day), the historical period (31.09 Joules/cm²/day), and the third future period (31.2 Joules/cm²/day). In the comparison between the historical period and the future periods (under the SSP585 scenario), the annual average radiation values, in ascending order, correspond to the first future period (30.69 Joules/cm²/day), the second future period (30.84 Joules/cm²/day), the third future period (30.85 Joules/cm²/day), and the historical period (31.09 Joules/cm²/day). The average radiation in the future 60-year statistical period under the SSP126 scenario increases by 0.11 Joules/cm²/day compared to the historical period. However, under the SSP245 and SSP585 scenarios, it decreases by 0.12 and 0.29 Joules/cm²/day, respectively, compared to the historical 30-year statistical period. The reason for the decrease in direct radiation to the Earth's surface could be an increase in water vapor and air humidity, or the scattering and absorption of sunlight by aerosols in the future. Additionally, as the Earth's relative distance from the Sun increases, the energy

received and the intensity of solar radiation will decrease.

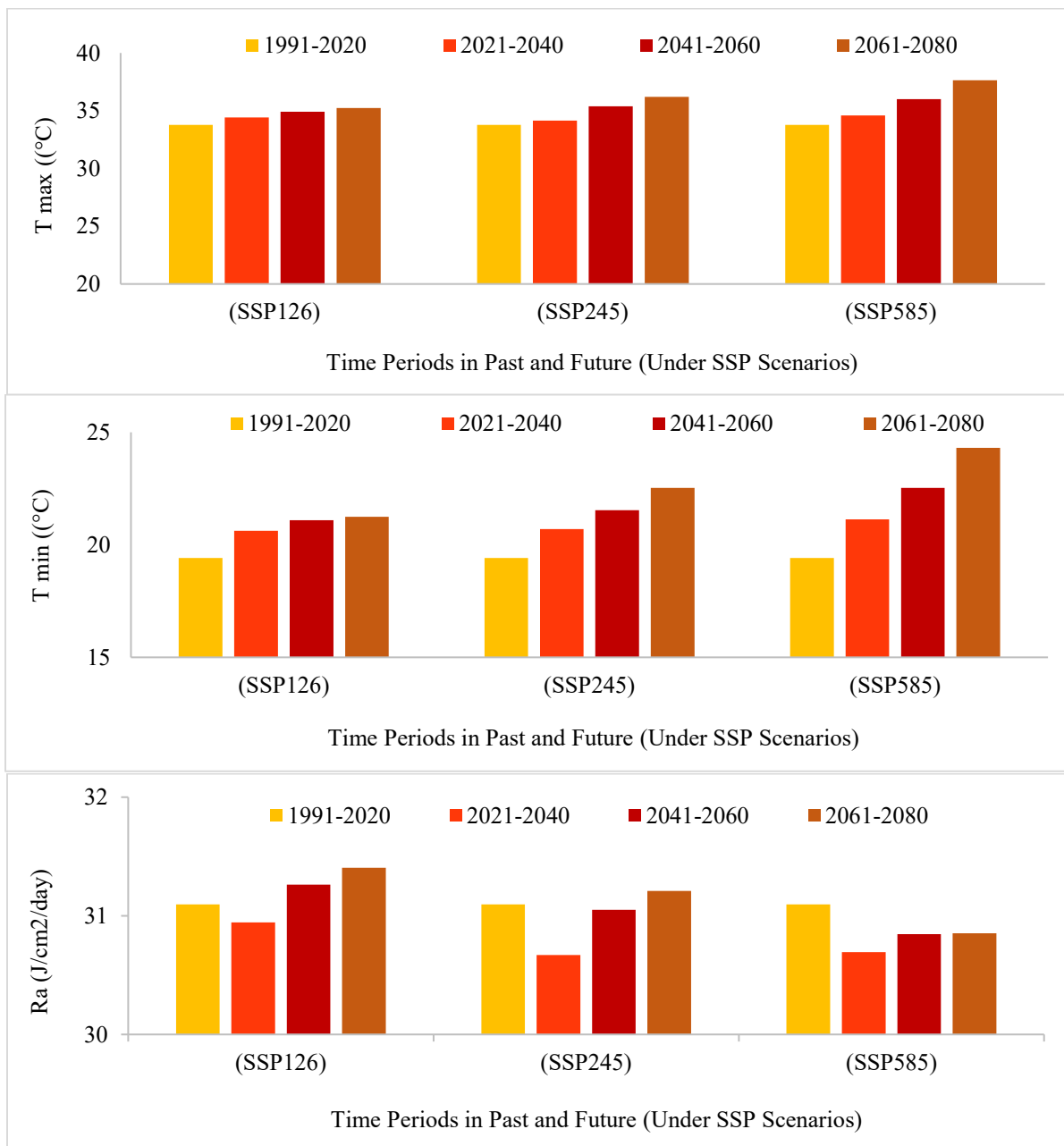


Figure 3. Trends in annual mean maximum temperature, minimum temperature, and solar radiation over historical and future periods (under SSP scenarios) in Ahvaz

Table 4 shows the trend in the monthly average climatic parameters of temperature and radiation at the Ahvaz station using the non-parametric Mann-Kendall test. The p-values for maximum temperature are less than 0.05 for all months of the year, which indicates a significant increasing

trend at the 95% confidence level. The minimum temperature, with the exception of February and March, exhibits a significant increasing trend at the 95% confidence level. In the comparison between the historical and future periods (under the SSP scenarios), the monthly average

maximum and minimum temperatures for all months are higher in the future periods than in the historical period.

In the comparison between the maximum temperature of the historical period and the future periods (under the SSP126, SSP245, and SSP585 scenarios), the highest maximum temperature belongs to August of the third future period (48.68, 49.79, and 51.58 °C, respectively), while the lowest maximum temperature occurs in January of the historical period (18.33 °C), the first future period (17.67 °C), and the first future period (18.03 °C) under SSP126, SSP245, and SSP585, respectively. In the comparison between the minimum temperature of the historical period and the future periods (under the SSP126,

SSP245, and SSP585 scenarios), the highest minimum temperature belongs to July of the third future period (32.2, 33.25, and 34.86 °C, respectively). The lowest minimum temperature is observed in January of the historical period (7.93 °C).

The trend in radiation is significant at the 95% confidence level only in March, April, May, July, and August; however, in the other months, no significant trend is observable, as the p-value for the maximum and minimum temperature parameters is greater than 0.05. The monthly trend of radiation at this station is inconsistent in the future periods compared to the historical period.

Table 4- Analysis of Monthly Trends in Climatic Parameters: Comparison of Future and Historical Periods in Ahvaz Using the Non-parametric Mann-Kendall Test

Month	Tmax		Tmin		Ra	
	p-Value	Z	p-Value	Z	p-Value	Z
Jan	0.022	0.234	0.022	0.234	0.066	0.179
Feb	0.022	0.234	0.017	0.234	0.066	0.179
Mrc	0.022	0.244	0.022	0.201	0.022	0.234
Apr	0.017	0.244	0.043	0.244	0.017	0.244
May	0.017	0.244	0.017	0.245	0.043	0.201
June	0.017	0.245	0.017	0.245	0.053	0.19
July	0.017	0.245	0.017	0.245	0.034	0.212
Aug	0.017	0.245	0.017	0.245	0.022	0.234
Sep	0.017	0.245	0.017	0.244	0.074	0.174
Oct	0.017	0.245	0.017	0.245	0.074	0.174
Nov	0.017	0.245	0.017	0.245	0.074	0.174
Dec	0.022	0.234	0.017	0.244	0.053	0.234

3.2.3. Kermanshah Station

The annual average maximum temperature, minimum temperature, and radiation for the past period and future periods under SSP scenarios for the Kermanshah station are shown in Figure 4. In general, the annual average maximum temperature in the future periods under all SSP scenarios is higher than that of the past period (23.97 °C). For the future periods, the annual average maximum temperature under the SSP126 scenario is 24.76, 25.37, and 25.7 °C for the first, second, and third periods, respectively. The annual average maximum temperature under the SSP245 scenario is 24.48, 25.9, and 26.77 °C for the first, second, and third future periods, respectively. Also, the annual average maximum temperature under the SSP585 scenario is 25.11, 26.38, and 28.35 °C for the first, second, and third

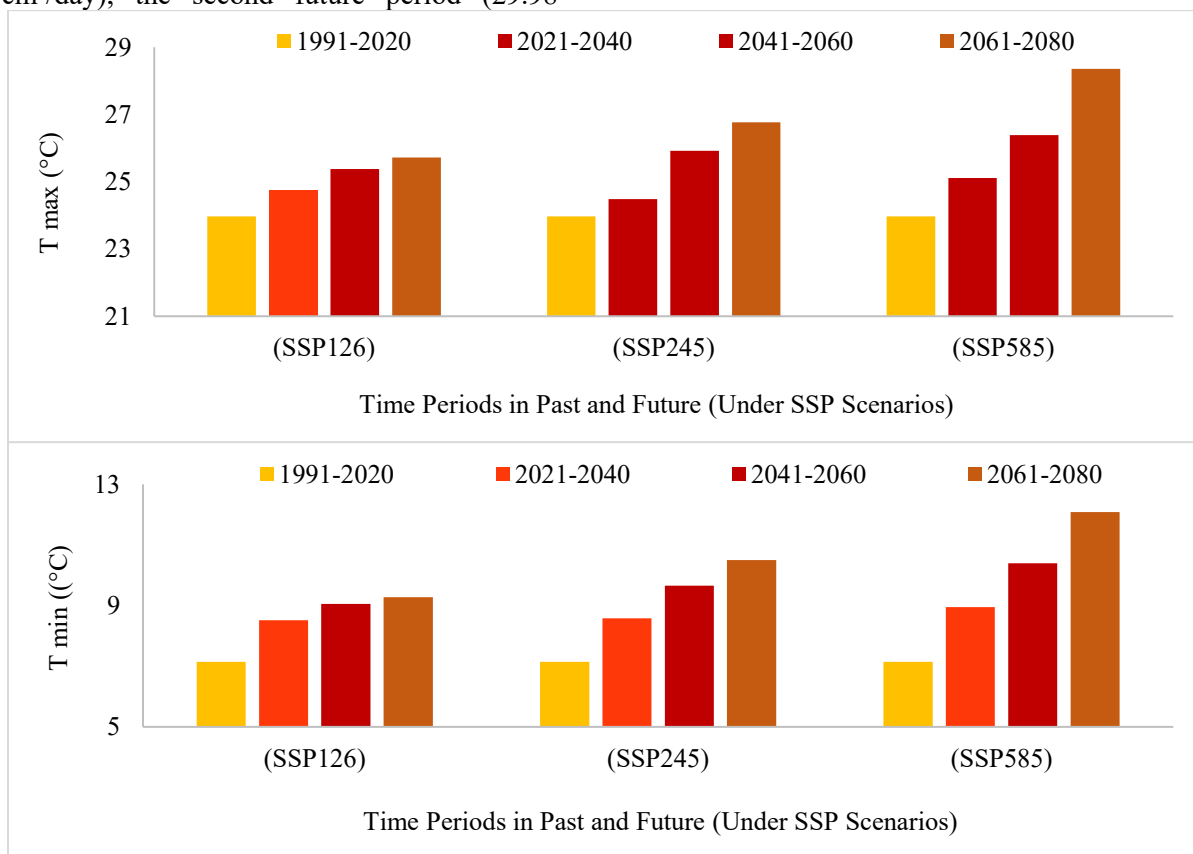
periods, respectively. The average maximum temperature in the future 60-year statistical period under the SSP126, SSP245, and SSP585 scenarios is projected to be 1.3, 1.75, and 2.65 °C higher, respectively, than in the past 30-year statistical period.

In general, the annual average minimum temperature in the future periods under all SSP scenarios is higher than that of the past period (7.14 °C). For the future periods, the annual average minimum temperature under the SSP126 scenario is 8.5, 9.06, and 9.27 °C for the first, second, and third periods, respectively. The annual average minimum temperature under the SSP245 scenario is 8.58, 9.65, and 10.49 °C for the first, second, and third future periods, respectively. Also, the annual average minimum temperature under the SSP585 scenario is 8.95,

10.39, and 12.08 °C for the first, second, and third periods, respectively. The average minimum temperature in the future 60-year statistical period under the SSP126, SSP245, and SSP585 scenarios is 1.8, 2.43, and 3.33 °C higher, respectively, than in the past 30-year statistical period.

In a comparison between the past period and the future periods (under the SSP126 scenario), the annual average radiation, in ascending order, corresponds to the first future period (29.94 J/cm²/day), the second future period (30.05 J/cm²/day), the past period (30.17 J/cm²/day), and the third future period (30.27 J/cm²/day). In a comparison between the past period and the future periods (under the SSP245 scenario), the annual average radiation, in ascending order, corresponds to the first future period (29.52 J/cm²/day), the second future period (29.98

J/cm²/day), the third future period (30.16 J/cm²/day), and the past period (30.17 J/cm²/day). In a comparison between the past period and the future periods (under the SSP585 scenario), the annual average radiation, in ascending order, corresponds to the first future period (29.67 J/cm²/day), the second future period (29.78 J/cm²/day), the third future period (30.045 J/cm²/day), and the past period (30.17 J/cm²/day). Compared to the past 30-year statistical period, the average radiation in the future 60-year statistical period decreases by 0.09, 0.28, and 0.33 J/cm²/day under the SSP126, SSP245, and SSP585 scenarios, respectively. The likely reason for the reduced solar radiation could be the formation of fewer but larger clouds due to the reduction of aerosols.



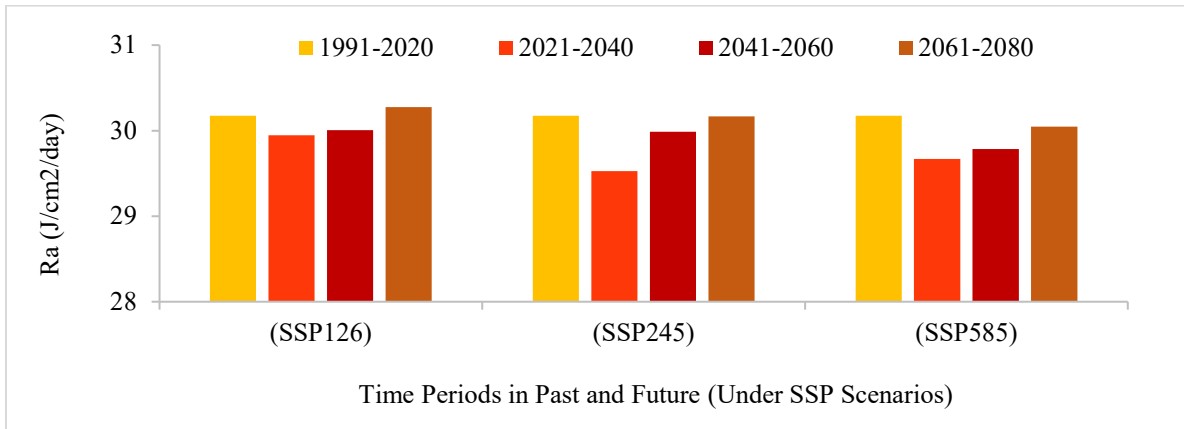


Figure 4. Trends in annual mean maximum temperature, minimum temperature, and solar radiation over historical and future periods (under SSP scenarios) in Kermanshah

Table 5 shows the trends in the monthly average of the climatic parameters—temperature and radiation—at the Kermanshah station, using the non-parametric Mann-Kendall test. The p-values for all three parameters—maximum temperature, minimum temperature, and radiation—are less than 0.05 for all months of the year, thus indicating a significant increasing trend at the 95% confidence level.

In a comparison between the past and future periods (under the SSP scenarios), the monthly average maximum and minimum temperatures for the city of Kermanshah were higher in the future periods than in the past period for nearly all months. In the city of Kermanshah, comparing the maximum temperature of the past period with the future periods (under the SSP126, SSP245, and SSP585 scenarios), the highest maximum temperature occurs in August of the third future period (40.78, 41.88, and 43.57 °C, respectively), and the lowest maximum temperature belongs to January of the first future period (8.59, 7.92, and 8.88 °C, respectively). In a comparison between the minimum temperature of the past period and

the future periods (under the SSP126, SSP245, and SSP585 scenarios), the highest minimum temperature belongs to July of the third future period (19.89, 21.26, and 22.87 °C, respectively). The lowest minimum temperature is observed in January of the past period (-3.02 °C).

The trend of monthly changes in radiation in this city for future periods, compared to past periods, was not consistent. According to a study by Zohrevandi et al. (2020), temperature and radiation in Kermanshah, as simulated by the HadCM3 General Circulation Model under the A1B, A2, and B1 scenarios, showed an increasing trend for future periods (2046-2065 and 2080-2099) compared to the baseline period (1961-2005). Similarly, BayatVarkeshi and Fasihi (2018) reported that, after studying the climatic conditions of 30 synoptic stations across the country, the forecast of meteorological parameters indicates a future increase in temperature and solar radiation at the national level. The results of the present study are consistent with the findings of previous research.

Table 5- Analysis of Monthly Trends in Climatic Parameters: Comparison of Future and Historical Periods in Kermanshah Using the Non-parametric Mann-Kendall Test

Month	Tmax		Tmin		Ra	
	p-Value	Z	p-Value	Z	p-Value	Z
Jan	0.022	0.234	0.022	0.234	0.043	0.201
Feb	0.017	0.245	0.022	0.234	0.027	0.223
Mrc	0.017	0.245	0.022	0.212	0.031	0.217
Apr	0.017	0.234	0.034	0.244	0.043	0.216
May	0.022	0.244	0.017	0.244	0.022	0.216
June	0.017	0.244	0.017	0.244	0.017	0.244
July	0.017	0.244	0.017	0.244	0.043	0.201
Aug	0.017	0.244	0.017	0.244	0.034	0.212
Sep	0.017	0.244	0.017	0.245	0.034	0.212
Oct	0.017	0.244	0.017	0.245	0.022	0.234
Nov	0.017	0.244	0.017	0.245	0.034	0.212
Dec	0.022	0.234	0.022	0.234	0.043	0.201

In both past and future periods, the maximum and minimum temperatures in Ahvaz are significantly higher than in Mashhad and Kermanshah. Therefore, when comparing the different regions, it is expected that Ahvaz will be at a greater risk of desertification in the future than the other cities. This can be attributed to its geographical location, topography, air currents from neighboring countries (Saudi Arabia and Iraq), lack of vegetation, and other factors. In this study, there is no significant difference in the amount of radiation (for different periods) among the studied climatic regions.

Based on the forecasting of future temperatures and radiation in this research, the future temperature development at the Mashhad, Ahvaz, and Kermanshah stations may result in higher evaporation of sea and river surfaces, thereby challenging freshwater resources. Moreover, temperature fluctuations lead to the melting of snow and ice, which will likely result in increased flooding in the future. In addition to these, erosion, a decrease in soil water, and changes in chemical composition and soil diversity are also consequences of future temperature rises. Hence, plant development and growth, as well as their crop yield and water demand, will also be influenced by future climate change.

4. Conclusions

In this research, the LARS WG8 software was utilized to project temperature and radiation at the Mashhad, Ahvaz, and Kermanshah stations. Initially, the accuracy of the HadGEM3 climate

model was validated. Subsequently, the projected changes in temperature and radiation for future periods (2021–2040, 2041–2060, and 2061–2080) under the SSP scenarios from the HadGEM3 model were compared with those of the historical period (1991–2020).

The results indicated that, for the studied stations, the annual mean maximum and minimum temperatures are projected to rise in future periods (under all SSP scenarios) relative to the historical period. However, the trend of changes in radiation was inconsistent compared to the historical period.

Among the implications of rising temperatures in the study areas for future periods are increased evaporation and declining water levels in seas and rivers; the melting of snow and ice; reduced watershed runoff and intensified drought; soil salinization and a decline in soil quality and fertility; increased plant water requirements and decreased crop yields; and the degradation of ecosystems and the environment. Changes in radiation also play a significant role in plant activities, such as photosynthesis, as well as in industry and the production of power and energy. Therefore, investigating the changing trends of temperature and radiation in future periods, particularly in study stations located in arid and semi-arid climates, can provide significant assistance to farmers, planners, and decision-makers in the management of water and soil resources, agriculture, watershed management, the environment, natural resources, and the economic sector. Developing suitable strategies

for the future will facilitate adaptation to new climatic conditions and mitigate potential damage. These strategies include, but are not limited to, the following:

- Planting more heat-tolerant crops.
- Designing appropriate watershed management systems.
- Optimal irrigation management, including the use of pressurized and innovative irrigation systems.
- Amending the soil and preserving soil moisture using organic matter (e.g., compost and mulch).
- Conservation measures and anti-desertification programs, such as cover planted to retain moisture, are essential.
- Installation of solar panels to ensure a sustainable energy supply.
- National and international cooperation and information exchange with other countries to combat climate change.

Furthermore, it is recommended that the projection of temperature and radiation for other arid and semi-arid regions of Iran, which have not yet been investigated, be conducted in the future using more up-to-date climate models and scenarios.

Author Contributions:

Marzieh Bagheri Khaneghahi: Conceptualization, performing software/statistical analyses, writing the original draft of the manuscript.

Aboutaleb HezarJaribi: Supervised, edited, and reviewed the manuscript and validation of the results.

Mohammad Ismaeil Kamali: Conceptualization, consultation, reviewing the manuscript, and statistical analysis.

Fatemeh Zamani: Consultation, reviewing the manuscript.

Conflicts of interest:

The authors of this paper declare that they have no conflict of interest regarding the writing and publication of the content and results of this research.

Data availability statement:

As the necessary data and information for this research were obtained from the Iran Meteorological Organization, the data used in this study cannot be made available.

References:

- Al-Kakey, O., Al-Mukhtar, M., Berhanu, S., & Dunger, V. (2023). Assessing CFSR climate data for rainfall-runoff modeling over an ungauged basin between Iraq and Iran. *Kuwait Journal of Science*, 50(3), 405–414. doi: 10.1016/j.kjs.2022.12.004
- Araya, A., Prasad, P. V. V., Gowda, P. H., Djanaguiramana, M., & Gebretsadkan, Y. (2021). Modeling the effects of crop management on food barley production under a midcentury changing climate in northern Ethiopia. *Climate Risk Management*, 32, 100308. doi: 10.1016/j.crm.2021.100308
- Bayatvarkeshi, M., & Fasihi, R. (2018). The analysis of downscaling results of weather parameters for Iran's future. *Geography and Environmental Sustainability*, 8(26), 87–73. https://ges.razi.ac.ir/article_898.html?lang=e [In Persian].
- Chen, H., Sun, J., Lin, W., & Xu, H. (2020). Comparison of CMIP6 and CMIP5 models in simulating climate extremes. *Science Bulletin*, 65(17), 1415–1418. doi: 10.1016/j.scib.2020.05.015
- Clarke, B., Otto, F., Stuart-Smith, R., & Harrington, L. (2022). Extreme weather impacts of climate change: An attribution perspective. *Environmental Research: Climate*, 1, 012001. doi: 10.1088/2752-5295/ac6e7d
- Dai, A. (2011). Drought under global warming: A review. *Wiley Interdisciplinary Reviews: Climate Change*, 2(1), 45–65. doi: 10.1002/wcc.81
- Dai, A. (2013). Increasing drought under global warming in observations and models. *Nature Climate Change*, 3, 52–58. doi: 10.1038/nclimate1633
- Dantas, L. G., dos Santos, C. A. C., Santos, C. A. G., Martins, E. S. P. R., & Alves, L. M. (2022). Future changes in temperature and precipitation over Northeastern Brazil by the CMIP6 model. *Water*, 14, 4118. doi: 10.3390/w14244118

- Haider, S., Masood, M. U., Rashid, M., Alshehri, F., Pande, C. B., Katipoğlu, O. M., & Costache, R. (2023). Simulation of the potential effects of projected climate and land use change on runoff under CMIP6 scenarios. *Water*, 15(19), 3421. doi: 10.3390/w15193421
- Hajivand Paydari, S., Yazdanpanah, H., & Andarzian, S. B. (2022). Investigation of regional effects of climate change phenomenon in the north of Khuzestan province using the HadCM3 model under LARS-WG exponential comparison in the statistical period of 2030–2010 and 2050–2030. *Journal of Geography and Human Relations*, 5(1), 299–314. doi: 10.22034/gahr.2022.330821.1669
- IPCC. (2012). Managing the risks of extreme events and disasters to advance climate change adaptation. (C. B. Field et al., Eds.). Cambridge University Press. <https://www.ipcc.ch/report/managing-the-risks-of-extreme-events-and-disasters-to-advance-climate-change-adaptation/>
- IPCC. (2013). Climate change 2013: The physical science basis. Contribution of Working Group I to the Fifth Assessment Report of the Intergovernmental Panel on Climate Change (T. F. Stocker et al., Eds.). Cambridge University Press. <https://www.ipcc.ch/report/ar5/wg1/>
- Iranshahi, M., Ebrahimi, B., Yousefi, H., & Moridi, A. (2022). Investigating the effects of climate change on temperature and precipitation using neural network and CMIP6 (Case Study: Aleshtar and Khorramabad stations). *Journal of Water and Irrigation Management*, 12(4), 821–845. doi: 10.22059/jwim.2022.346796.1009
- Lionello, P., & Scarascia, L. (2018). The relation between climate change in the Mediterranean region and global warming. *Regional Environmental Change*, 18(5), 1481–1493. doi: 10.1007/s10113-018-1290-1
- Mahmoudi, P., & Rigi Chahi, A. (2019). Climate change's impact on the spatial and temporal distribution of precipitation in Iran. In 6th International Regional Conference on Climate Change (pp. 1–12), Tehran, Iran. <https://www.researchgate.net/publication/337427637>
- Moghadas, P., Mahjoobi, E., & Gharechelou, S. (2024). Prioritization of the CMIP6 general circulation models using multi-criteria decision-making methods in the Nekarood watershed. *Iranian Journal of Irrigation and Drainage*, 18(1), 15–25. https://idj.iaid.ir/article_183799.html?lang=fa [In Persian].
- Mosayyebi, M. (1996). Climate change and its effects on the ecosystems of arid and semi-arid areas. *Quarterly Scientific-Research Journal of Geographic Information*, 5(16), 42–46. https://www.sepehr.org/article_29309.html
- Muhaisen, N. K. H., Khayyun, T. S., Al Mukhtar, M., & Hassan, W. H. (2024). Forecasting changes in precipitation and temperatures of a regional watershed in Northern Iraq using LARS-WG model. *Open Engineering*, 14, 20220567. doi: 10.1515/eng-2022-0567
- Munawar, S., Rahman, G., Moazzam, M. F. U., Miandad, M., Ullah, K., Al-Ansari, N., & Linh, N. T. T. (2022). Future climate projections using SDSM and LARS-WG downscaling methods for CMIP5 GCMs over the Transboundary Jhelum River Basin of the Himalayas Region. *Atmosphere*, 13, 898. doi: 10.3390/atmos13060898
- Navarro-Racines, C. (2020). High-resolution and bias-corrected CMIP5 projections for climate change impact assessments. *Scientific Data*, 7, 7. doi: 10.1038/s41597-019-0343-8
- Osman, Y., Al-Ansari, N., Abdellatif, M., Aljawad, S. B., & Knutsson, S. (2014). Expected future precipitation in central Iraq using LARS-WG stochastic weather generator. *Engineering*, 6(13), 948–959. doi: 10.4236/eng.2014.613086
- Qin, P., Xu, H., Liu, M., Liu, L., Xiao, C., Mallakpour, I., & Sorooshian, S. (2022). Projected effects of climate change on major dams in the Upper Yangtze River Basin. *Climatic Change*, 170(1–2), 8. doi: 10.1007/s10584-021-03303-w
- Sarabi, M., Dastorani, M. T., & Zarrin, A. (2020). Investigating impact of future climate changes on temperature and precipitation condition (Case Study: Torogh Dam Watershed, Mashhad). *Journal of Meteorology and Atmospheric Sciences*, 3(1), 63–83. doi:

- 10.22034/jmas.2021.278862.1129 [In Persian].
- Semenov, M. A., & Barrow, E. M. (2002). LARS-WG: A stochastic weather generator for use in climate impact studies (Version 3.2) [User's manual].
<https://www.researchgate.net/publication/268304865>
- Semenov, M. A., & Stratonovitch, P. (2009). The use of multi-model ensembles from global climate models for impact assessments of climate change. *Climate Research*, 41, 1–14.
- Shoja, F., & Hamidianpour, M. (2024). Projection influences of climate change on tourism development on the southern coast (Kish Island). *Journal of Tourism and Development*, 12(37), 237–255. doi: 10.22034/jtd.2023.380876.2725 [In Persian].
- Tang, J., Niu, X., Wang, S., Gao, H., Wang, X., & Wu, J. (2016). Statistical downscaling and dynamical downscaling of regional climate in China: Present climate evaluations and future climate projections. *Journal of Geophysical Research: Atmospheres*, 121(5), 2110–2129. doi: 10.1002/2015JD023977
- Trenberth, K. E., Dai, A., van der Schrier, G., Jones, P. D., Barichivich, J., Briffa, K. R., & Sheffield, J. (2014). Global warming and changes in drought. *Nature Climate Change*, 4, 17–22. doi: 10.1038/nclimate2067
- Zamani, Y., Hashemi Monfared, S. A., Azhdari Moghaddam, M., & Hamidianpour, M. (2020). A comparison of CMIP6 and CMIP5 projections for precipitation to observational data: The case of northeastern Iran. *Theoretical and Applied Climatology*, 142, 1613–1623. doi: 10.1007/s00704-020-03406-x
- Zohrevandi, H., Khorshiddost, A. M., & Sari Saraf, B. (2020). Prediction of climate change in Western Iran using downscaling of HadCM3 model under different scenarios. *Journal of Spatial Analysis Environmental Hazards*, 7(1), 49–64. <http://jsaeh.khu.ac.ir/article-1-2741-fa.html> [In Persian].